CrystEngComm

Two structurally diverse Zn-based coordination polymers with excellent antibacterial activity

Journal:	*CrystEngComm*
Manuscript ID	CE-ART-03-2018-000394.R1
Article Type:	Paper
Date Submitted by the Author:	22-May-2018
Complete List of Authors:	Colinas, Ian; University of California, Santa Cruz, Department of Chemistry and Biochemistry Rojas-Andrade, Mauricio; University of California, Department of Chemistry and Biochemistry Chakraborty, Indranil; University of California, Department of Chemistry Oliver, Scott; University of California, Santa Cruz, Department of Chemistry and Biochemistry

Journal Name

ARTICLE

Two structurally diverse Zn-based coordination polymers with excellent antibacterial activity

Received 00th January 20xx,
Accepted 00th January 20xx

DOI: 10.1039/x0xx00000x

www.rsc.org/

Ian R. Colinas,[a] Mauricio D. Rojas-Andrade,[a] Indranil Chakraborty[b] and Scott R. J. Oliver[a,*]

We report the synthesis and antibacterial properties and mechanism of two Zn-based coordination polymers (CPs). The first, $[Zn(bipy)(OH_2)_4^{2+}]_{1.5}[ClO_4^-]_3 \bullet (bipy)_3(H_2O)$, consists of a one-dimensional (1D) structure with two crystallographically independent octahedral zinc centers trans-coordinated by two 4,4'-bipy units and water groups. The second, $[Zn_{1.5}(CH_3CO_2)_2(bipy)_2^+][ClO_4^-] \bullet H_2O$, is a two-dimensional (2D) layered structure with the same polymers but bridged together into a layer by acetate and 4,4'-bipy. Both compounds exhibit sustained release of Zn^{2+} ions upon their gradual degradation in aqueous solution, which results in highly effective antibacterial activity towards *Escherichia coli* and particularly towards *Staphylococcus epidermidis* cells. This activity was evaluated in solution by broth dilution assays to determine minimal inhibition concentrations (MICs) as well as in the solid phase by agar diffusion tests to quantify the zones of inhibition (ZOI), and were in close agreement. Further, the biocidal mechanisms of the coordination polymers were investigated *in vivo* by fluorescence microscopy utilizing CellRox Green and propidium iodide as reactive oxygen species (ROS) and membrane disruption indicators, respectively. Both CPs show superior antibacterial activity compared to two standards, zinc acetate and zinc oxide, which is concluded to be due to both gradual and localized release of Zn^{2+} ions as well as electrostatic attraction to the bacterial cell surface afforded by their unique structures. This unique Zn release profile and interaction with bacterial surfaces affords marked antibacterial activity and suggests that manipulation of the Zn structures could lead to significant advancements in antimicrobial materials.

1. Introduction

Increasing antibiotic resistance of pathogens has become a serious threat to public health. The spread of these resistant pathogens is occurring at a faster rate than the discovery of new antibacterial agents, contributing to the recent rise of untreatable infections.[1] It is estimated that more than two million people in the United States are infected with resistant bacteria annually, with over 23,000 deaths as a direct result.[2] Given that both intrinsic and acquired bacterial resistances are mediated by genetic pathways such as mutations in chromosomal genes in response to exposure of the cell to an antibacterial agent, new strategies to develop materials with effective, broad-spectrum antibacterial activity are needed in order to mitigate genetic bacterial resistance.[3]

An effective approach to control the spread of antibiotic resistant bacteria is to consider a material that exhibits this broad-spectrum biocidal activity both in liquid environments, and on solid surfaces. Infectious bacteria are most commonly found in a sessile state in the form of a biofilm, rather than in a planktonic or free-swimming form. This biofilm is responsible for adhesion of bacteria to surfaces and plays a significant role in the transmission of antibiotic-resistant infections.[4] Hence, the fabrication of new materials that can be used for prophylactic purposes, such as surface treatment of surgical tools and implanted medical devices, as well as more common surfaces such as door handles, light switches, and countertops could prove to be an effective strategy to prevent the growth of biofilms and, in turn, the spread of antibiotic resistant infections.

The antimicrobial use of metals such as silver (Ag), gold (Au), cobalt (Co), copper (Cu) and zinc (Zn) has been widely studied and applied for centuries.[5,6,7,8] Recently, the field of nanotechnology has incorporated these metals into nanostructured systems for improved dosage forms and therapeutic effects.[9,10] Unlike conventional antibiotics, the antibacterial activity of nanomaterials is broad-spectrum, and includes physical damage to bacterial cells. These mechanisms typically involve the release of toxic metal ions and formation of reactive oxygen species (ROS). The affinity of these metal ions for biomolecules as well as their ability to generate ROS result in a variety of toxic effects, including altered membrane permeability, loss of proton motive force, leakage of cellular contents, and arrest of DNA replication.[11] Among these metal containing nanomaterials, silver is the most widely used

[a] Address here. Department of Chemistry and Biochemistry, University of California, Santa Cruz, 1156 High Street, Santa Cruz, California 95064
[b] Chemistry and Biochemistry Florida International University, MMC 11200 SW 8th Street (CP-304) Miami, Florida 33199.
† Footnotes relating to the title and/or authors should appear here.
Electronic Supplementary Information (ESI) available: [details of any supplementary information available should be included here]. See DOI: 10.1039/x0xx00000x

bioactive metal due to the interaction of silver ions with multiple cellular targets, conferring its broad spectrum activity against bacterial cells.[12,13,14,15] The main drawback of Ag compounds and nanostructures however, are their relatively high cost and the limited solubility of Ag^+ in the presence of chloride ions [$K_{sp}(AgCl) = 1.77 \times 10^{-11}$]. Cl^- ions are a common species in bacterial habitats and inside bacterial cells, causing precipitation of Ag^+ and adversely affecting nanoparticle aggregation and dissolution kinetics.[16,17]

In contrast, zinc is a low cost, endogenous transition metal whose chloride complex has a strong thermodynamic propensity for hydration.[18,19] Zinc has been incorporated in various compounds for a wide range of applications such as antimicrobial agents and treatment of Alzheimer's disease.[20,21,22] In an effort to understand the toxicity of zinc ions towards bacteria, Paton *et al.* performed both *in vivo* and *in vitro* analyses with *Streptococcus pneumoniae*.[23] The authors revealed that extracellular Zn(II) inhibits the acquisition of Mn(II) by gram-positive bacterial cells by competitive binding via the solute-binding protein PsaA. Their studies demonstrated that this extracellular cation competition can occur for several pathogenic and non-pathogenic bacteria, resulting in oxidative stress due to starvation of essential Mn(II). The antimicrobial effect of ZnO nanoparticles on gram-negative *E. coli* cells has also been demonstrated in a study by Brayner et *al.*[24] They found that ZnO nanoparticles exerted their biocidal activity by damaging the cell membrane through cellular internalization, the degree of which was governed by the nature of the capping ligand. These studies shed light on the mechanisms of zinc-based structures' bactericidal properties, and demonstrate their efficacy for antimicrobial applications, prompting further investigation to achieve additional improvements.

Although highly effective, ZnO nanoparticles require a passivating agent to prevent their aggregation[25] which can be detrimental[24] to the antibacterial activity. Therefore, a material that provides stoichiometric release of biocidal metal ions without aggregation would be an ideal platform for antibacterial Zn-based materials. Metal-organic frameworks (MOFs), more generally known as coordination polymers (CPs), are an emerging class of materials with wide diversity of topologies and properties which is afforded by the plethora of metal centers and organic linkers used to design them. The structure of a CP is tunable by synthetic factors such as the coordination geometry of the metal center, the nature of the ligand as well as counter anions, their molar ratios, and synthetic conditions such as temperature or solvent system.[26] Although these hybrid materials have been traditionally investigated for applications in gas storage,[27] sensing,[28] separation,[29] and drug delivery,[30] they have recently demonstrated interesting antibacterial activity.

The antibacterial properties typically originate from the metals in their cationic form, with the structures acting as metal ion reservoirs. Both the organic linkers and ions residing in the pores, however, may contribute to the antibacterial activity.[11] For instance, the biocidal activity of a Zn-based MOF was previously demonstrated to result from the additive effect of Zn^{2+} and azelate moiety which acted as a bioactive linker for the Zn^{2+} nodes.[31] This MOF demonstrated successful inhibition of *S. aureus* and *S. epidermidis* growth by its progressive release of Zn^{2+} ions and azelaic acid. The biocidal mechanisms of each of these moieties however, was not thoroughly addressed, leaving the exact roles of these two bactericidal species unsolved.

Herein, we report the hydrothermal synthesis of two zinc-based CPs, $[Zn(bipy)(OH_2)_4^{2+}]_{1.5}[ClO_4^-]_3 \cdot (bipy)_3(H_2O)$ (which we denote SLUG-39, for University of California, Santa Cruz, Structure, No. 39) and $[Zn_{1.5}(C_2H_3O_2)_2(bipy)_2^+][ClO_4^-] \cdot H_2O$ (SLUG-40). Both consist of Zn^{2+} ions as the metal nodes connected by 4,4'-bipyridine linkers, SLUG-39 forms a one-dimensional (1D) structure with two crystallographically independent octahedral zinc centers trans-coordinated by two 4,4'-bipy units and water groups, while SLUG-40 is a two-dimensional (2D) layered structure with the same polymers but bridged together into a layer by acetate and 4,4'-bipy. We detail their synthesis, characterization, and provide an in-depth evaluation of their biocidal activity against gram-negative (E. coli) and gram-positive bacteria (S. epidermidis).

2. Experimental

2.1 Materials

Zinc nitrate hexahydrate [$Zn(NO_3)_2 \cdot 6H_2O$, Fisher, 99.5%], zinc acetate dihydrate [$Zn(CH_3CO_2)_2 \cdot 2H_2O$, Mallinckrodt chemicals, 98%], sodium perchlorate monohydrate [$NaClO_4 \cdot H_2O$, Fluka, 98%], 4,4'-bipyridine [$C_{10}H_8N_2$, Acros, 98%] and Miller Luria broth (Fisher) were all used as-received. Water was supplied by a Barnstead Nanopure water system (18.3 MΩ•cm).

2.2 Synthesis of SLUG-39

A mixture of $Zn(NO_3)_2 \cdot 6H_2O$ (1.4 mmol), $NaClO_4 \cdot H_2O$ (1.4 mmol) and 4,4'-bipyridine (2.8 mmol) was stirred mildly for 1 h in 10 mL of H_2O, then sealed in a 15 mL Teflon-lined stainless steel autoclave and heated at 150 °C for 20 h under autogenous pressure. Large white needles were isolated under vacuum filtration and subsequently rinsed with deionized water and acetone (yield: 0.34 g, 60.9% based on 4,4'-bipy). Elemental analysis (Galbraith Laboratories, Inc.): C, 44.27% (44.11% theoretical); H: 3.88% (4.08% theoretical); N: 10.28% (10.29% theoretical). FT-IR (cm^{-1}): 1615, 1600, 1536 (m, $\nu_{C=N}$), 1490, 1418 (m, $\nu_{C=C}$), 1095 (s, ν_{ClO4-}), 812 (m, ν_{C-H}), 509 (m, ν_{Zn-O}), 476 (m, ν_{Zn-N}).

2.3 Synthesis of SLUG-40

A mixture of $Zn(CH_3CO_2)_2 \cdot 2H_2O$ (1.4 mmol), $NaClO_4 \cdot H_2O$ (1.4 mmol) and 4,4'-bipyridine (2.8 mmol) was stirred mildly for 1 h in 10 mL of H_2O, then sealed in a 15 mL Teflon-lined stainless steel autoclave and heated to 150 °C for 20 h under autogenous pressure. Yellow tan flake crystals were isolated under vacuum filtration and subsequently rinsed with deionized water and acetone [yield: 0.46 g, 70.8% based on $Zn(OAc)_2$]. Elemental analysis (Galbraith Laboratories, Inc.): C,

43.72% (44.62% theoretical); H: 3.70% (3.745% theoretical); N: 8.68% (8.43% theoretical). FT-IR (cm^{-1}): 1605, 1581(m, $\nu_{C=N}$), 1408 (m, ν_{C-O}-), 1064 (s, ν_{ClO4}-), 812 (m, ν_{C-H}), 510(m, ν_{Zn-O}), 479 (m, ν_{Zn-N}).

2.4 Characterization

Single crystal data for SLUG-39 and SLUG-40 were recorded using a Bruker APEX II CCD area detector X-ray diffractometer with graphite monochromated Mo-Kα radiation (λ = 0.71073 **Å**). The structures were solved by direct methods and expanded routinely. The models were refined by full-matrix least-squares analysis of F^2 against all reflections. All non-hydrogen atoms were refined with anisotropic thermal displacement parameters. Hydrogen atom positions were calculated geometrically and refined isotropically using the riding model. TwinRotMat function within *PLATON* program indeed suggested a twin law for SLUG-39 crystal data. This structure was re-refined against an hklf5 file. PXRD for both structures was measured on a Rigaku Americas Miniflex Plus diffractometer, scanning from 2 to 40° (2θ) at a rate of 2°/min with a 0.04° step size under Cu-Kα radiation (λ = 1.5418 **Å**). Thermogravimetric analysis (TGA) was performed on a TA Instruments TGA Q500 by heating from 25 to 600 °C under N_2 purge with a gradient of 5 °C/min. Elemental analysis (CHN) was performed on a EAI CE-440 elemental analyzer. A PerkinElmer Spectrum-One FT-IR spectrometer was used to obtain the IR spectra of the compounds.

2.5 Quantification of Zn^{2+} Release

Samples of SLUG-39 and SLUG-40 were ground and immersed in distilled water at 37 °C at a concentration of 100 ppm. Aliquots of the supernatant solution were initially taken in triplicate trials every 20 min, and then every 24 h for the first 4 days. The Zn^{2+} concentration was determined by Inductively Coupled Plasma-Optical Emission Spectroscopy (ICP-OES) using a Perkin-Elmer Optima 7000 DV ICP-OES instrument.

2.6 Growth Inhibition Assay

Antibacterial properties of as-synthesized SLUG-39 and SLUG-40 were evaluated against *Escherichia coli* (ATCC# 25922) and *Staphylococcus epidermidis* (ATCC# 12228) using similar methodology as previously reported by Rojas-Andrade et al.[12] All experiments were performed with fresh bacteria grown by first spreading frozen liquid culture on a Luria broth (LB) agar plate and incubating at 37 °C for 24 h. A single colony was isolated and used to inoculate 3 mL of LB. The bacterial culture was incubated for 18 h at 37 °C under constant shaking at 250 rpm. A 1 mL aliquot of this bacterial culture was then placed in a 1.5 mL microcentrifuge tube and centrifuged at 5000 rpm for 5 min. The obtained pellet was subsequently re-suspended in 1 mL of sterile nanopure water and this process was repeated an additional two times. Enough of the final re-suspended pellet was added to 5 mL of Nanopure water to adjust its absorbance to 0.100 at 600 nm, referred as the optical density (OD600). Minimum inhibitory concentrations (MIC) were obtained by performing broth dilution experiments in triplicates. For these experiments, a 96-well plate was utilized, each well filled with 30 µL of sterile LB, 10 µL of the 0.1 OD600 bacterial suspension, varying amounts (100, 90, 80, 70, 60, 50 and 40 µL) of the antimicrobial material and enough Nanopure water to bring the final volume to 200 µL. The final concentration of the antimicrobial agents was determined based on total zinc content. Once the wells were inoculated and all components added, the 96-well plate was immediately placed in a Molecular Devices VERSAmax microplate reader and the optical density for each well was measured at 600 nm every 5 min over the 24 h incubation period, with 10 s mixing periods between reads at 37 °C.

2.7 Agar Diffusion Tests

The bacterial inoculums were prepared in a similar fashion as above, with the final suspension adjusted to 0.100 optical density. A 100 µL aliquot of this suspension was then placed on the surface of each LB agar plate and evenly spread using silica glass beads. The antibacterial agents were then placed on top of the agar plates in the form of a circular pellet consisting of 70% KBr and 30% sample and evaluated based on their total zinc content using a pure KBr pellet as a control. The zone of inhibition (ZOI) diameter for each sample was measured with a vernier caliper after a 24 h incubation period at 37 °C, which was also performed in triplicates.

2.8 Fluorescence Microscopy

The suspensions of *Escherichia coli* and *Staphylococcus epidermidis* used for imaging were prepared by rinsing overnight liquid cell cultures with nanopure water as described above, excluding the final dilution to 0.100 optical density. The rinsed suspension was then incubated with 5 µM CellROX Green and 10 µM propidium iodide for 30 min in the dark. These dye-incubated cells were then centrifuged and re-suspended in 100 µL of antimicrobial materials, from which a 2 µL drop was taken and placed onto a microscope cover slip (0.17 mm thickness) for fluorescence imaging. A Solamere Spinning disk confocal microscope equipped with a Nikon TE2000 inverted stand, a CSU-X1 spinning disk and a Hamamatsu Image EMX2 camera using Micro-manager software was utilized to obtain all images. A 60x Nikon Plan Apo was utilized as the objective lens. A 488 nm laser with a 500-550 nm band-pass emission filter, and a 561 nm laser with a 573-613 nm band pass filter were used as the excitation sources for CellROX Green and propidium iodide respectively. Bacterial suspensions were imaged at 1 frame per second for a total of 10 min with 100 ms exposure time for each laser.

3. Results and Discussion

3.1 Structural Properties of SLUG-39

Large white needle crystals of SLUG-39 were obtained by the hydrothermal reaction of zinc nitrate in the presence of 4,4-bipy and perchlorate ions at 150 °C (Figure S1). The crystal structure of SLUG-39 was authenticated by single crystal X-ray diffraction and both the asymmetric unit and the crystal packing pattern are shown in Figures S2 and 1, respectively. PXRD of the as-synthesized SLUG-39 confirms the material is

single phase and matches the theoretical pattern based on the single-crystal solution (Figure S3). This coordination polymer crystallizes in a triclinic form with a space group P-1 (Table 1). The two crystallographically independent Zn^{2+} centers have an octahedral coordination environment, with four terminal water molecules in a square-planar arrangement. Two trans nitrogens from two μ-2 bridging 4,4'-bipy units complete the coordination sphere, forming a cationic secondary building unit counterbalanced by two perchlorate groups. The two Zn^{2+} centres and 4,4'-bipy linkers form chains (Figure 1), which are separated by perchlorate anions and perpendicular π-stacked pairs of 4,4'-bipy. The 4,4'-bipy pairs are found in two different conformations, both exhibiting π-stacking (3.420 to 3.750 Å). Several moderate classical hydrogen bonding interactions consolidated the extended lattice of SLUG-39. Some notable interactions are, O(coordinated H_2O)-H---N(bpy), with O---N, 2.723(8), 2.714(8), 2.740(8) Å; O(coordinated H_2O)-H---O(ClO_4), with O---O, 2.808(8) and 2.914(13) Å; O(lattice H_2O)-H---O(coordinated water), with O---O, 2.726(9) and 2.877(11) Å

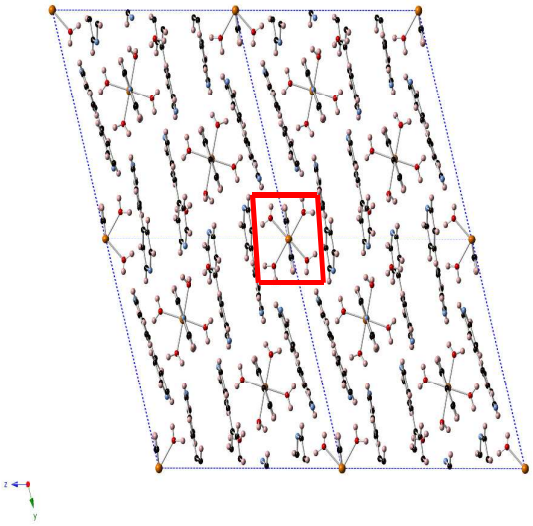

Figure 1. Crystal packing pattern of SLUG-39 showing the water-terminated polymeric chains end-on (one example is outlined in red) that propagate along the *x* direction; free perchlorate and water molecules are omitted for clarity (Zn: orange; N: blue; O: red; C: black; H: white).

Three perchlorate molecules counterbalance the cationic chains by electrostatic interactions that result in long Zn-O distances of 4.223(1) and 4.555(7) Å. The perchlorates also provide additional stability *via* hydrogen bonding interactions with three Zn-coordinated water groups (Figure S4). Other coordination polymers with coplanar 4,4'-bipy units include $Co(NCS)_2(H_2O)_2$(4,4'-bipy)·4,4'-bipy[32] and Zn(4,4'-bipy)$_2(H_2O)_2SiF_6$.[33] Finally, a crystallographically identified non-coordinated water resides between the perchlorate groups, further stabilizing the structure by hydrogen bonding to a coordinated water group [O···H-O distance 1.917(1) Å].

Thermogravimetric analysis (Figure S5) confirms the presence of occluded water in the structure by the initial mass loss of 1.5% around 30 °C, followed by a ~ 9.0% (8.8% theoretical) mass loss corrresponing to the coordinated water groups around 120 °C. The next event corresponds to a two-step decomposition of the 4,4'-bipy groups, in which an initial 1.5 molar equivalents decompose at ~ 210 °C representing an 18.5% mass loss (19.1% theoretical). Finally, the decomposition of the 3.0 molar equivalents of interlamellar 4,4'-bipy units occurs at ~ 300 °C, accounting for a 39% mass loss (38.2% theoretical).[32]

The IR spectrum confirms the presence of both the polymeric and free interchain 4,4'-bipy units in the structure (Figure S6). We attribute the aromatic C=N stretches at 1605 and 1535 cm^{-1} to the linking units and the additional stretch at 1617 cm^{-1} to the uncoordinated units.[34] The presence of perchlorate is verified by the characteristic stretch at 1095 cm^{-1} and the coordination of zinc can be seen by the low frequency stretch at 476 cm^{-1} due to the Zn-N bond.[26]

3.2 Structural Properties of SLUG-40

Small tan flake crystals of SLUG-40 were obtained by the hydrothermal reaction of zinc acetate in the presence of 4,4'-bipy and perchlorate at 150 °C (Figure S7). In contrast to SLUG-39, SLUG-40 is a two-dimensional cationic MOF due to the acetate of the zinc reagent rather than nitrate. There are two unique Zn centres. Zn(1) has a trigonal bipyramidal geometry axially coordinated by two 4,4'-bipy units, resulting in an infinite polymeric chain with alternating Zn and 4,4'-bipy units in the crystallographic *b*-direction (Figure 2a). Zn(1) is coordinated along [10-1] by an additional μ-2 4,4'-bipy that further bridges two Zn(1) centers of neighboring polymers, as well as two η-2 bridging acetates that connect Zn(1) to Zn(2). In contrast, Zn(2) is octahedral, coordinated by two 4,4'-bipy units, giving rise to infinite connectivity along the *b*-direction (Figure S8). The other four coordination sites of Zn(2) correspond to the aforementioned bridging acetates that connect two Zn(1) centers along [10-1] (Figure 2b). The four acetate groups allows for Zn(2) to bridge two Zn(1) centers, giving rise to a layer of repeated Zn(1)-Zn(2)-Zn(1) trimer units (red box, Figure 2b). These three polymers are thus parallel and the neighboring 4,4'-bipy units are π-stacked with distances of 3.525(1) and 3.787(1) Å along [10-1]. The perchlorate anions reside in the channels and counterbalance the cationic chains [Zn-O distances 5.341(1) and 5.469(1) Å]. PXRD of the as-synthesized SLUG-40 confirms the material is single phase and matches the theoretical pattern based on the single-crystal solution (Figure S9). No classical hydrogen bonding interactions have been noted for SLUG-40 structure.

The IR data confirms the two coordination environments around the two zinc centres. The C-O^- stretch at 1408 cm^{-1} corresponds to the acetate bridging ligand and the low frequency stretches at 510 and 409 cm^{-1} correspond to Zn-O and Zn-N, respectively (Figure S10).[26] In addition, the C=N stretches at 1605 and 1581 cm^{-1} are attributed to the 4,4'-bipy units. The perchlorate anions counter-balancing the cationic

structure are confirmed by the characteristic singlet stretch at 1061 cm^{-1}. Thermogravimetric analysis (Figure S11) reveals an initial mass loss of ~ 2.5% at 85 °C, corresponding to the occluded water (2.5% theoretical). The acetate bridging groups are lost around 200 °C, with ~ 19.2% mass loss (18.4% theoretical). Finally, a two-step occurs where 0.5 molar equivalents of the 4,4'-bipy units are evolved at ~ 220 °C, accounting for a 14.2 % mass loss (12.1 % theoretical). Finally,1.5 molar equivalents of the 4,4'-bipy units decompose at ~ 320 °C with 34.3% mass loss (36.2% theoretical).

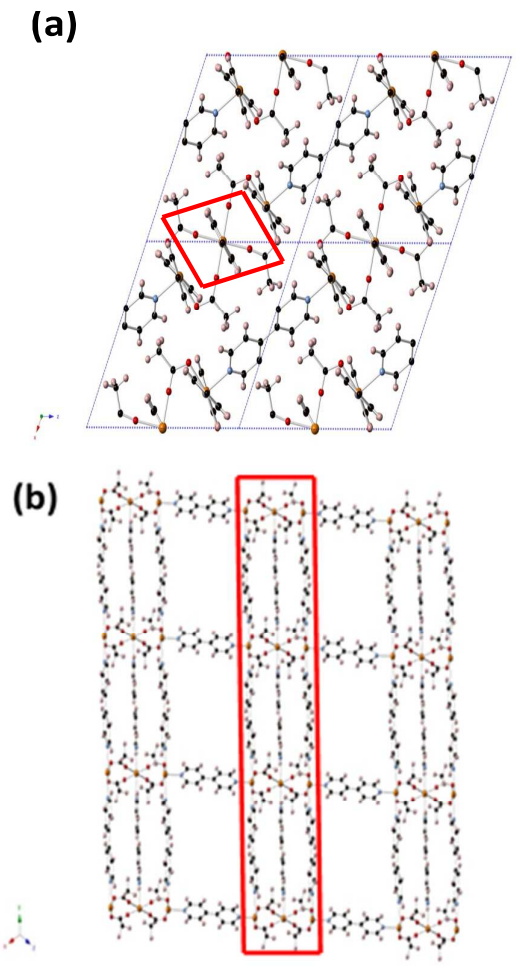

Figure 2. (a) Crystal packing pattern structure of SLUG-40 showing polymeric chains along the y-axis with perchlorate and water molecules omitted for clarity; (b) Crystal packing pattern of one layer of the SLUG-40 framework. The red outline highlights one set of three parallel, acetate-bridged polymers.

3.3 Zn^{2+} Release Profiles

One advantage of a material that can release Zn^{2+} ions upon contact with fluids compared to the other bioactive metal ions such as Ag^{+} is the high solubility of the Zn^{2+} in the presence of common ions such as chlorides. This greater solubility

Table 1. Crystal data and structure refinement of SLUG-39 and SLUG-40.

	SLUG-39	**SLUG-40**
empirical formula	$C_{45}H_{50}Cl_3N_9O_{19}Zn_{1.5}$	$C_{24}H_{24}ClN_4O_9Zn_{1.5}$
formula weight (g/mol)	1225.34	645.98
wavelength (Å)	0.71073 Mo-Kα	0.71073 Mo-Kα
crystal system	triclinic	triclinic
space group	P-1	P-1
unit cell dimensions	*a* = 11.314(6) Å *b* = 15.217(9) Å *c* = 17.158(10) Å α =106.412(7) ° β = 98.879(6) ° γ = 105.061(6) °	*a* = 11.3806(10) Å *b* = 11.4717(10) Å *c* = 11.9184(10) Å α =105.855 (1) ° β = 108.975(1) ° γ = 101.196(1) °
volume ($Å^3$)	2652(3)	1345.2(2)
Z, calculated density (g/cm^3)	2, 1.534	2, 1.595
absorption coefficient (mm^{-1})	0.917	1.510
crystal size (mm)	0.06 x 0.18 x 0.20	0.15 x 0.20 x 0.25
color of crystal	white	tan
θ range for data collection (deg)	2.5 - 25.0	2.8 - 24.7
index ranges	-12≤ h ≤13, -18≤ k ≤17, -20≤ l ≤ 20	-13 ≤ h ≤ 13, -13≤ k ≤ 13, -13 ≤ l ≤ 13
completeness to θ	89.7% (θ = 25.097)	98.0% (θ = 24.709)
collected/unique reflections	12113/8480 [R(int) = 0.034]	9444/4493 [R(int) = 0.017]
absorption correction	semi-empirical	semi-empirical
max. and min. transmission	0.745 and 0.623	0.745 and 0.599
refinement method	full-matrix least-squares on F^2	full-matrix least-squares on F^2
refls / restraints / parameters	8480/ 23 / 738	4493 / 0 / 363
goodness of fit on F^2	1.030	1.040
R indices	R_1 = 0.067, wR_2 = 0.182	R_1 = 0.060, wR_2 = 0.141
Largest diff. peak and hole	0.80 and -0.85 ($e/Å^{-3}$)	1.71 and -1.54 ($e/Å^{-3}$)

maintains elevated concentrations of biocidal ions in the environment and allows these ions to make contact with bacterial cells more efficiently. In order to evaluate the ability of both SLUG-39 and SLUG-40 to release ions upon contact with relevant fluids, the degradation of both coordination polymers was investigated in aqueous media at 37 °C. This degradation is expressed as the % Zn^{2+} released compared to the total Zn present in the coordination polymer solid.

Careful inspection of the release of Zn^{2+} ions was performed by taking aliquots of the supernatant solution in both 20 min and 1 d intervals and subsequently determining their respective concentrations by ICP-OES. In the first 2 h (Figure 3a), SLUG-39 exhibits a significantly greater Zn^{2+} release rate than SLUG-40, with approximately 50 % of Zn^{2+} ions released into solution. The faster release of ions can be

attributed to the lower stability of the one-dimensional coordination polymer, held together primarily by hydrogen bonding and weaker π-stacking interactions. Conversely, SLUG-40 exhibits a more sustained release of ions, releasing only *ca*. 15% of the Zn^{2+} ions in the first 2 h. The slower release of Zn^{2+} ions from SLUG-40 stems from its higher dimensionality layered structure, in which the zinc polymers are found as trimeric units compared to the discrete polymers coordinated by four terminal water groups in SLUG-39. Interestingly, the long-term release of ions for both coordination polymers equalizes after 4 d at ~ 83 % release (Figure 3b). Hence, both SLUG-39 and SLUG-40 can serve as reservoirs of Zn^{2+} ions and have ion release profiles that are suitable for different applications. SLUG-39, which exhibits relatively fast ion release, may be suitable for hospital fixtures or surgical devices that require rapid sterilization upon contact, while SLUG-40 with its slower ion release may be applicable in medical implants and cosmetic products.

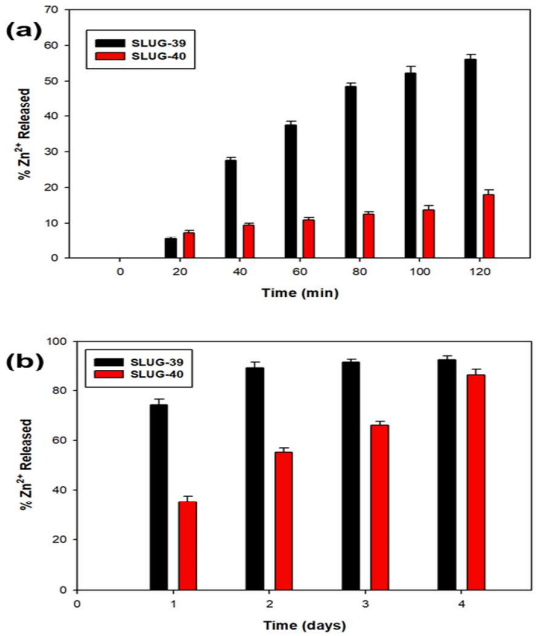

Figure 3. Zinc ion release profiles of SLUG-39 and SLUG 40 in distilled water at 37 °C over (a) 120 min and (b) 4 d time intervals.

3.4 Antibacterial Assays

The antibacterial properties of the as-synthesized coordination polymers were evaluated against both gram-positive (*Staphylococcus epidermidis*) and gram-negative (*Escherichia coli*) strains. Initially, the biocidal activity of SLUG-39, SLUG-40 and relevant controls was quantified by monitoring the growth of bacterial cultures in liquid media over a 24 h period in the presence of varying concentrations of each biocidal species. Growth curves for both *E. coli* and *S. epidermidis* grown in the presence of each zinc CP as well as with zinc acetate are shown in Figure 4. Further, 4,4'-bipy and sodium perchlorate were also investigated to determine their contribution to the biocidal activity of the coordination polymers, but interestingly, no inhibitory effect was observed from these components (Figure S12).

Due to the difference in zinc composition of the two coordination polymers, their concentrations were normalized to their overall zinc content, allowing for the determination of the minimum inhibitory concentration (MIC) in terms of zinc concentration (Table 2). The MIC represents the concentration at which no bacterial growth is observed during the incubation period, as indicated by the lack of optical density at 600 nm above the baseline value. Based on these growth curves, it is evident that both SLUG-39 and SLUG-40 exhibited an enhanced inhibitory effect on the growth of E. coli and S. epidermidis with respect to the zinc acetate control. In the case of E. coli, SLUG-39 and SLUG-40 displayed an MIC of 5.3 and 6.1 ppm, respectively, markedly lower than $Zn(OAc)_2$ which only showed complete inhibition above 7.7 ppm. Interestingly, MIC values were found to be lower against S. epidermidis, with SLUG-39, SLUG-40, and $Zn(OAc)_2$ demonstrating MICs of 3.8, 4.6 and 4.6 ppm, respectively. Further, the lag-phase (T_L) durations were determined from the bacterial growth curves to obtain more insight from the growth kinetics. This value represents a measure of the work required for a bacterial colony to adapt to its environment, and it is defined as the as the time between inoculation and initiation of the log phase. As seen on figure S13, the lag-phase durations of the both SLUG-39 and SLUG-40 are noticeably longer than that of zinc acetate due to the bacterial cells requiring longer periods of time to achieve optimal conditions for replication.

These results are in agreement with previous findings[20,35,36] and suggests Staphylococcus species are more susceptible to zinc toxicity, contrary to the traditionally accepted activity based on differences between gram-positive and gram-negative cell wall structures. Indeed, gram-positive cell walls consist of a much thicker layer of peptidoglycan than gram-negative cell walls, typically affording enhanced protection from environmental stressors compared to gram-negative.[37] Due to the unique chemistry of the Zn^{2+} ion however, the constituents of gram-positive cell walls—teichioic acids (TA) and lipoteichioic acids (LTA), which makeup a significant fraction of the overall mass, are more susceptible to damage by this species. Zn^{2+} ions are known to catalyze the hydrolysis of esters[38,39], phosphodiesters[40] and amides[41], all of which are structurally significant functional groups in both TA/LTA and peptidoglycan biomolecules. Therefore, the enhanced activity towards S. epidermidis can reasonably be attributed to the membrane damage caused by Zn^{2+} species resulting from the degradation of the CP. This damage may occur as a result of the catalytic hydrolysis of phosphodiester and amide bonds that make up the backbones of TA/LTA molecules, which may crosslink with peptidoglycan units. Gram-negative E. coli cells on the other hand, have an extra (outer) membrane which contain molecules of lipopolysaccharide (LPS) that acts as a hydrophobic barrier against Zn^{2+} ions. This barrier cannot be

readily disrupted by Zn^{2+} ions as these molecules lack ester and phosphodiester linkages between the subunits of their structure, and instead have glycosidic bonds, for which Zn^{2+} species are ineffective at cleaving.[42] In fact, it has been shown that divalent cations act to electrostatically crosslink LPS molecules, transforming the outer-membrane into a low-permeability barrier which could serve to protect the cell.[43]

In addition, the Zn^{2+} ions can exert their toxicity by competition for essential extracellular cations, i.e. Mn^{2+}, which may lead to oxidative stress.[23,44] Although all three samples are sources of Zn^{2+}, the two CPs still demonstrated lower MICs than zinc acetate (6.9 ppm), a standard free form of Zn^{2+} ions.

This result indicates that the coordination polymers have additional structural properties that attribute them a higher antibacterial activity. This greater activity can be due to both their gradual Zn^{2+} release as well as their Zn^{2+} coordination structure. Upon contact with water, the CPs take on a net positive charge that is likely attracted to the net negatively-charged bacterial cell surfaces, affording localized release of Zn^{2+} ions. Bipyridine ligands have been previously incorporated into complexes as well as studied on their own for their biocidal activity. Their observed activity was concluded to arise from both its metal coordinating behavior as well as its ability to make cells aggregate.[45,46,47] Hence, the 4,4'-bipy units may synergistically add to the biocidal activity by facilitating the aggregation of cells around the CPs, further localizing and concentrating Zn^{2+} ions around bacterial cells. In fact, it has been reported that the antimicrobial effect of Zn^{2+} ions on E. coli is dependent on the concentration as well as the contact duration, which plays a significant role in the biocidal activity, as is the case with our two CPs.[21]

The antibacterial activity of the coordination polymers was also investigated in their solid form by performing agar diffusion tests and determining the resultant zones of inhibitions. In order to accurately compare the activity of each of the antibacterial agents, the diameters of inhibition zones were normalized to total zinc content of the structure (Figure 5). Similar results were obtained for E. coli and S. epidermidis, with SLUG-39 exhibiting the largest ZOI, followed by SLUG-40. Both demonstrated superior activity to $Zn(OAc)_2$ and especially ZnO. Further, *S. epidermidis* exhibited a higher susceptibility to the biocidal effects of Zn antibacterial agents than *E. coli*, in agreement with the broth dilution assays.

Table 2. MIC values of SLUG-39, SLUG-40 and the $Zn(OAc)_2$.

Compound	*E. coli* MIC (ppm)*	*S. epidermidis* MIC (ppm)*
SLUG-39	5.3	3.8
SLUG-40	6.1	4.6
$Zn(OAc)_2$	6.9	4.6

* Concentration in terms of overall zinc content.

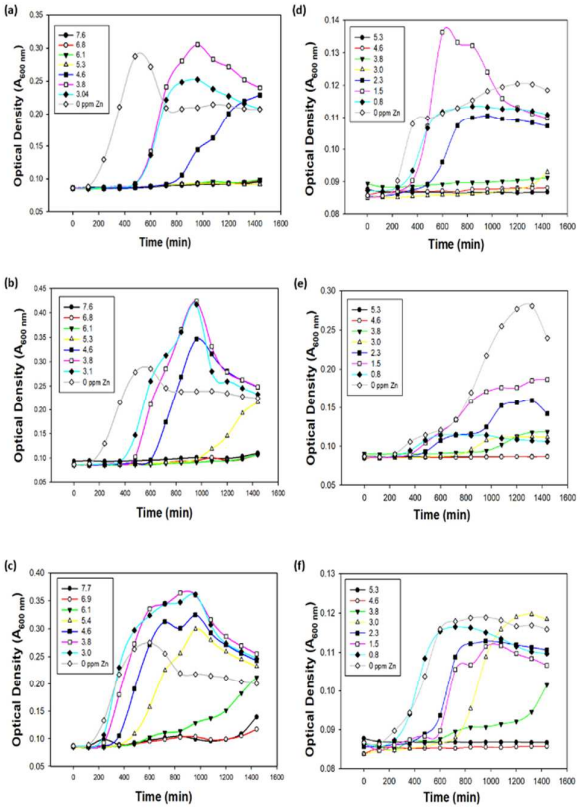

Figure 4. Growth curves of E. Coli (a-c) and S. Epidermidis (d-f) in the presence of SLUG-39 (a,d), SLUG-40 (b,e), and $Zn(OAc)_2$ (c,f) at varying concentrations.

The superior activity from the CPs compared to zinc acetate and ZnO is likely due to a combination of gradual and sustained release of Zn^{2+} ions from the slow degradation of these crystalline materials as well as their mobility through the agar media. Upon degradation, SLUG-39 forms long chains which likely have a much higher mobility through the pores of the agar than the 2-D layers of SLUG-40 accounting for the observed differences in ZOI. Unlike the highly soluble zinc acetate salt that leads to immediate dissolution and sequestering of Zn^{2+} ions by the functional groups of the agar substrate, the gradual release from the CPs provides a more localized and concentrated form of biocidal Zn^{2+} ions. This

localization likely enhances internalization into bacterial cells, leading to enhanced disruption of membrane structure and cation homeostasis.[48,49] ZnO was observed to exhibit the lowest inhibition for both bacterial strains due to its low solubility in aqueous environments. In addition, the activity of the individual components of the CPs as well as a KBr control were investigated. Of these, only the 4,4'-bipy ligand exhibited a zone of inhibition (Figure S14), which was relatively minimal compared with the other samples. This result suggests the linker alone does not contribute significantly to the biocidal activity, which is also in agreement with the broth dilution experiments.

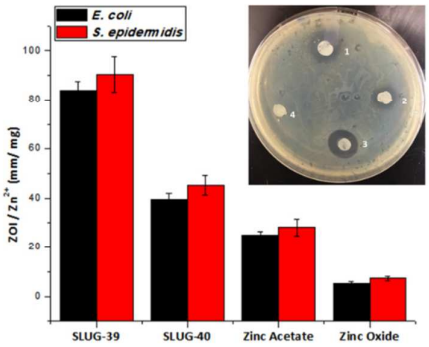

Figure 5. Bar chart of normalized zones of inhibition (ZOI) of E. coli and S. epidermidis, and photograph of a typical agar plate with E. coli lawn displaying ZOIs upon treatment with: (1) SLUG-39; (2) SLUG-40; (3) Zn(OAc)2; (4) ZnO.

3.5 Fluorescence Microscopy

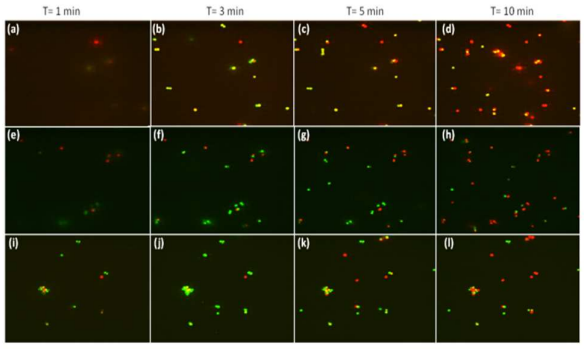

Figure 6. Fluorescence micrographs of *S. epidermidis* incubated with 5 µM CellROX Green and 10 µM propidium iodide and treated with: (a-d) SLUG-39; (e -h) SLUG-40; (i - l) $Zn(OAc)_2$ over a 10-minute period.

The mechanism of the biocidal activity that SLUG-39 and SLUG-40 demonstrate against *S. epidermidis* was further investigated *in vivo* utilizing fluorescence microscopy, with CellRox Green and propidium iodide. CellRox Green indicates the formation of hydroxyl radicals and superoxide anions which result from oxidative stress undergone by the cell emitting fluorescence at 520 nm. Propidium iodide is used to evaluate cell membrane integrity, as indicated by the fluorescence emission at 636 nm upon intercalation with DNA in the event of entry into bacterial cells due to membrane damage. Bacterial cells were suspended in freshly-prepared solutions of the coordination polymers or zinc acetate at a concentration of 15.2 ppm by zinc content, as well as pure water as a control. The cells resuspended in water demonstrated a minimal relative fluorescent cell count of both dyes over a period of 10 min (Figure S15).

Interestingly, however, treatment of *S. epidermidis* with SLUG-39, SLUG-40, and zinc acetate resulted in a pronounced increase in fluorescent cells, with a gradual change from green to red fluorescence observed over 10 minutes (Figure 6). The cells treated with zinc acetate initially exhibited the highest CellRox fluorescence cell count, with 3 and 6 times more green cells observed than SLUG-39 and SLUG-40, respectively (Figure 7a). This greater count indicates that a high level of oxidative stress was being caused in affected cells, likely due to the fast release of Zn^{2+} ions causing elevated ROS generation. This fast release likely results in a relatively high concentration of intercellular Zn^{2+}, causing rapid disruption of metabolic activity through extracellular cation competition, subsequently causing this oxidative stress. After three minutes of exposure, however, both CPs demonstrated a much more comparable number of green fluorescent cells. This observation correlates well with their zinc-release profiles and suggests the oxidative stress is directly related to free Zn^{2+}.

As the contact time increases, the cells begin experiencing membrane damage as seen by the gradual increase in the number of red fluorescing cells (Figure 7b). After the first minute, all samples have a similar percentage of red fluorescent cells. SLUG-39, however, observes the highest count of these cells at every time point proceeding, with both CPs observing higher counts than zinc acetate after 10 min. This higher count can be explained by the ability of the CP to wrap around and generally localize themselves to bacterial cell surfaces, with both the 4,4'-bipy units and the localized release of Zn^{2+} ions contributing to the enhanced membrane damage activity. SLUG-39, having both 4-4'-bipy and Zn^{2+} moieties that are easily released, optimally enhances interactions of CP units with bacterial cells and facilitates Zn^{2+} toxicity, respectively.

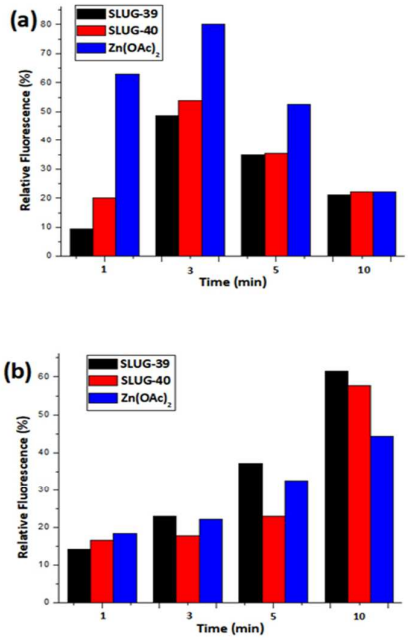

Figure 7. Relative fluorescence of *S. epidermidis* cells in the presence of SLUG-39 (black), SLUG-40 (red) and $Zn(OAc)_2$ (black), incubated with: (a) CellROX; (b) propidium iodide.

4. Conclusions

Two crystalline CP materials have demonstrated enhanced antibacterial activities in both liquid and solid growth media compared with typical Zn sources. *In vivo* studies utilizing fluorescence microscopy suggest that both materials induce cell death by oxidative stress and membrane damage resulting from Zn^{2+} toxicity. The enhanced biocidal properties of these CPs are likely due to gradual and localized release of Zn^{2+} ions, likely resulting from enhanced electrostatic interactions with bacterial cell surfaces afforded by their unique coordination structure. This study demonstrates how careful manipulation of zinc-based structures could provide low cost, Earth abundant and highly bioactive materials that are promising candidates for controlling bacterial growth in many situations such as in healthcare, cosmetic and food environments.

Conflicts of interest

The authors declare no competing financial interest.

Acknowledgements

This work was supported by the National Science Foundation under Grant No. 1603754 from the CBET Environmental Engineering GOALI Program. Ian R. Colinas was supported by a graduate fellowship from the Initiative for Maximizing Student Development (IMSD) program funded by the National Institutes of Health under Grant No. 5R25GM058903-18. We acknowledge Professor Chad Saltikov of the Department of Microbiology and Environmental Toxicology at UC Santa Cruz for his assistance and facilities used for bacterial cell viability studies. We would like to thank Dr. Bill Saxton and Dr. Susan Strome of the UC Santa Cruz MCD biology department for access to the microscopy facility, and Dr. Benjamin Abrams for technical assistance with the spinning disk confocal microscope.

References

1 L. L. Ling, T. Schneider, A. J. Peoples, A. L. Spoering, I. Engels, B. P. Conlon, A. Mueller, T. F. Schäberle, D. E. Hughes, S. Epstein, M. Jones, L. Lazarides, V. A. Steadman, D. R. Cohen, C. R. Felix, K. A. Fetterman, W. P. Millett, A. G. Nitti, A. M. Zullo, C. Chen and K. Lewis, *Nature*, 2015, **517**, 455–459.

2 World Health Organization, Ed., *Antimicrobial resistance: global report on surveillance*, World Health Organization, Geneva, Switzerland, 2014.

3 J. M. A. Blair, M. A. Webber, A. J. Baylay, D. O. Ogbolu and L. J. V. Piddock, *Nat. Rev. Microbiol.*, 2014, **13**, 42–51.

4 C. Wu, J. Labrie, Y. D. N. Tremblay, D. Haine, M. Mourez and M. Jacques, *J. Appl. Microbiol.*, 2013, **115**, 30–40.

5 Q. Feng, J. Wu, G.-Q. Chen, F.-Z. Cui, T. N. Kim and J. O. Kim, *A mechanistic study of the antibacterial effect of silver ions onEscherichia coli andStaphylococcus aureus*, 2000, vol. 52.

6 S. Uruş, O. Serindağ and M. Diğrak, *Heteroat. Chem.*, 2005, **16**, 484–491.

7 K. M. Patel, K. N. Patel, N. H. Patel and M. N. Patel, *Synth. React. Inorg. Met.-Org. Chem.*, 2001, **31**, 239–246.

8 A. Golcu, M. Tumer, H. Demirelli and R. A. Wheatley, *Inorganica Chim. Acta*, 2005, **358**, 1785–1797.

9 S. M. Dizaj, F. Lotfipour, M. Barzegar-Jalali, M. H. Zarrintan and K. Adibkia, *Mater. Sci. Eng. C*, 2014, **44**, 278–284.

10 A. J. Huh and Y. J. Kwon, *J. Controlled Release*, 2011, **156**, 128–145.

11 G. Wyszogrodzka, B. Marszałek, B. Gil and P. Dorożyński, *Drug Discov. Today*, 2016, **21**, 1009–1018.

12 M. Rojas-Andrade, A. T. Cho, P. Hu, S. J. Lee, C. P. Deming, S. W. Sweeney, C. Saltikov and S. Chen, *J. Mater. Sci.*, 2015, **50**, 2849–2858.

13 J. R. Morones, J. L. Elechiguerra, A. Camacho, K. Holt, J. B. Kouri, J. T. Ramírez and M. J. Yacaman, *Nanotechnology*, 2005, **16**, 2346–2353.

14 W.-R. Li, X.-B. Xie, Q.-S. Shi, H.-Y. Zeng, Y.-S. OU-Yang and Y.-B. Chen, *Appl. Microbiol. Biotechnol.*, 2010, **85**, 1115–1122.

15 Z. Lu, K. Rong, J. Li, H. Yang and R. Chen, *J. Mater. Sci. Mater. Med.*, 2013, **24**, 1465–1471.

16 X. Li, J. J. Lenhart and H. W. Walker, *Langmuir*, 2010, **26**, 16690–16698.

17 K. A. Huynh and K. L. Chen, *Environ. Sci. Technol.*, 2011, **45**, 5564–5571.

18 R. Pappalardo and E. Marcos, *J. Phys. Chem*, 1993, **97**, 4500–4504.

19 W. W. Rudolph and C. C. Pye, *Phys. Chem. Chem. Phys.*, 1999, **1**, 4583–4593.
20 A. Masoudiasl, M. Montazerozohori, R. Naghiha, A. Assoud, P. McArdle and M. Safi Shalamzari, *Mater. Sci. Eng. C*, 2016, **61**, 809–823.
21 A. A. Abdel Aziz, I. H. A. Badr and I. S. A. El-Sayed, *Spectrochim. Acta. A. Mol. Biomol. Spectrosc.*, 2012, **97**, 388–396.
22 J. Constantinidis, *Drug Dev. Res.*, 1992, **27**, 1–14.
23 C. A. McDevitt, A. D. Ogunniyi, E. Valkov, M. C. Lawrence, B. Kobe, A. G. McEwan and J. C. Paton, *PLoS Pathog.*, 2011, **7**, e1002357.
24 R. Brayner, R. Ferrari-Iliou, N. Brivois, S. Djediat, M. F. Benedetti and F. Fiévet, *Nano Lett.*, 2006, **6**, 866–870.
25 S.-W. Bian, I. A. Mudunkotuwa, T. Rupasinghe and V. H. Grassian, *Langmuir*, 2011, **27**, 6059–6068.
26 G.-C. Xu, L. Zhang, Y.-H. Zhang, J.-X. Guo, M.-Q. Shi and D.-Z. Jia, *CrystEngComm*, 2013, **15**, 2873.
27 K. Sumida, D. L. Rogow, J. A. Mason, T. M. McDonald, E. D. Bloch, Z. R. Herm, T.-H. Bae and J. R. Long, *Chem. Rev.*, 2012, **112**, 724–781.
28 A. Karmakar, B. Joarder, A. Mallick, P. Samanta, A. V. Desai, S. Basu and S. K. Ghosh, *Chem Commun*, 2017, **53**, 1253–1256.
29 R. Custelcean and B. A. Moyer, *Eur. J. Inorg. Chem.*, 2007, **2007**, 1321–1340.
30 J. R. Long and O. M. Yaghi, *Chem. Soc. Rev.*, 2009, **38**, 1213.
31 C. Tamames-Tabar, E. Imbuluzqueta, N. Guillou, C. Serre, S. R. Miller, E. Elkaïm, P. Horcajada and M. J. Blanco-Prieto, *CrystEngComm*, 2015, **17**, 456–462.
32 J. Lu, T. Paliwala, S. C. Lim, C. Yu, T. Niu and A. J. Jacobson, *Inorg. Chem.*, 1997, **36**, 923–929.
33 R. W. Gable, B. F. Hoskins and R. Robson, *J Chem Soc Chem Commun*, 1990, 1677–1678.
34 H. Fei, M. R. Bresler and S. R. J. Oliver, *J. Am. Chem. Soc.*, 2011, **133**, 11110–11113.
35 S. Atmaca and K. Gül, *Turk. J. Med. Sci.*, 1998, 595–597.
36 F. M. Aarestrup and H. Hasman, *Vet. Microbiol.*, 2004, **100**, 83–89.
37 T. J. Silhavy, D. Kahne and S. Walker, *Cold Spring Harb. Perspect. Biol.*, 2010, **2**, a000414–a000414.
38 J. Chin, *Acc. Chem. Res.*, 1991, **24**, 145–152.
39 R. M. Carrillo, A. G. Neo, L. López-García, S. Marcaccini and C. F. Marcos, *Green Chem*, 2006, **8**, 787–789.
40 S. Mikkola, I. Zagorowska and H. Lönnberg, *Nucleosides Nucleotides*, 1999, **18**, 1267–1268.
41 T. J. Przystas and T. H. Fife, *J. Chem. Soc. Perkin Trans. 2*, 1990, 393.
42 M. D. Leavell and J. A. Leary, *J. Am. Soc. Mass Spectrom.*, 2001, **12**, 528–536.
43 A. K. Chatterjee, H. Ross and K. E. Sanderson, *Can. J. Microbiol.*, 1976, **22**, 1549–1560.
44 M. Coelho Abrantes, M. de F. Lopes and J. Kok, *PLoS ONE*, 2011, **6**, e26519.
45 A. Rotaru, M. Ungureanu, R. Danac, A. Poeata and I. Druta, *Ann. Pharm. Fr.*, 2004, **62**, 428–430.
46 R. Kaushal, N. Kumar, P. Awasthi and K. Nehra, *Turk. J. Chem.*, 2013, **37**, 936–945.
47 M. C. Grenier, R. W. Davis, K. L. Wilson-Henjum, J. E. LaDow, J. W. Black, K. L. Caran, K. Seifert and K. P. C. Minbiole, *Bioorg. Med. Chem. Lett.*, 2012, **22**, 4055–4058.
48 J. Wątły, S. Potocki and M. Rowińska-Żyrek, *Chem. - Eur. J.*, 2016, **22**, 15992–16010.
49 J. Pasquet, Y. Chevalier, J. Pelletier, E. Couval, D. Bouvier and M.-A. Bolzinger, *Colloids Surf. Physicochem. Eng. Asp.*, 2014, **457**, 263–274.

TOC Synopsis:

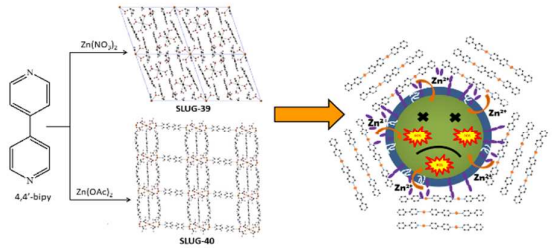

Two novel Zn-based coordination polymers with unique structural properties display an exceptional antibacterial activity against Gram-positive and Gram-negative bacteria.

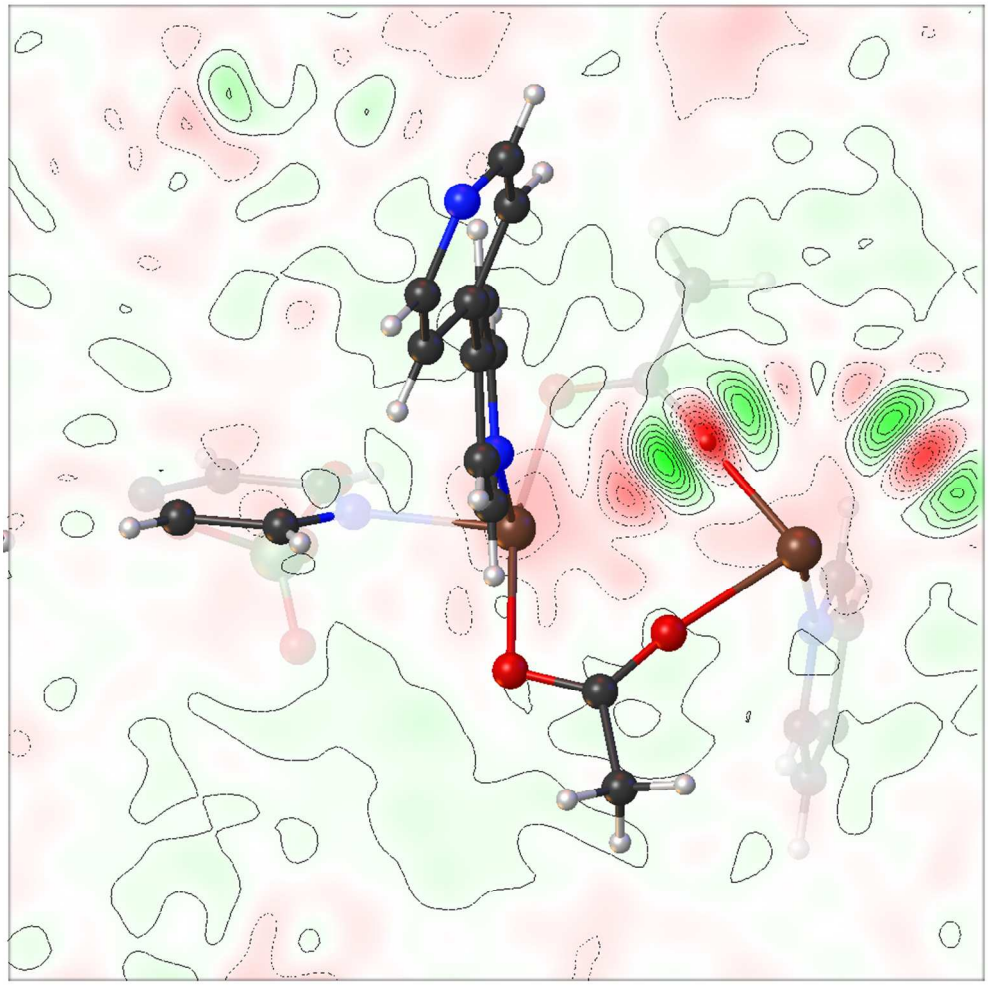

377x378mm (72 x 72 DPI)